General attached eddies: Scaling laws and cascade self-similarity

Ruifeng Hu [1,*] Siwei Dong [2,†] and Ricardo Vinuesa [3,‡]

[1] *Center for Particle-Laden Turbulence, Key Laboratory of Mechanics on Disaster and Environment in Western China, Ministry of Education, and College of Civil Engineering and Mechanics, Lanzhou University, Lanzhou 730000, China*

[2] *State Key Laboratory of Aerodynamics, Mianyang 621000, China*

[3] *FLOW, Engineering Mechanics, KTH Royal Institute of Technology, SE-100 44 Stockholm, Sweden*

(Received 9 December 2022; accepted 5 April 2023; published 24 April 2023)

The attached-eddy model (AEM) is one of the most successful coherent-structure-based phenomenological models in wall turbulence. In the classical AEM, the probability density of eddy p_e is assumed to follow an inverse law with the eddy size h_e, i.e., $p_e \propto h_e^{-1}$, to satisfy a constant Reynolds-shear-stress distribution in the inertial layer of canonical wall-bounded turbulent flows. In this paper, we first extend the AEM to general attached eddies with $p_e \propto h_e^{-\alpha}$, where α is an arbitrary positive real number. Scaling laws for velocity covariance (Reynolds stress) by general attached eddies are derived. Preliminary evidence for the validity of the model is provided from adverse-pressure-gradient turbulent boundary layer and turbulent wing boundary layer flows. Second, considering that the eddy cascade self-similarity is manifested by generalized power laws for probability density p_e, population density M_e, area coverage C_e, and volume fraction V_e of eddies, i.e., $p_e \propto h_e^{-\alpha}$, $M_e \propto h_e^{-\beta}$, $C_e \propto h_e^{-\gamma}$, and $V_e \propto h_e^{-\zeta}$, we directly connect the exponents with the fractal dimension D_e of the general attached eddies in a simple and clear way. The present paper highlights that the scaling laws of velocity covariance in the inertial layer of wall-bounded turbulent flows can be directly linked to the characteristics of the cascade self-similarity of the general attached eddies. We believe that the scaling laws derived here and the generalized power-law relationships are useful for a deeper understanding of the connection between coherent structures and turbulence statistics.

DOI: 10.1103/PhysRevFluids.8.044603

I. INTRODUCTION

Coherent-structure-based modeling of wall-bounded turbulent flow is an active topic in turbulence research and is far from maturity. The classical attached-eddy hypothesis (AEH) by Townsend [1], as well as the following attached-eddy model (AEM) [2–6], are some of the most celebrated kinematic and phenomenological models in wall turbulence [7]. We will use the term AEM in this paper to denote both AEH and AEM. In the AEM, a wall-bounded turbulent flow is modeled as a superposition of hierarchically self-similar wall-attached eddies populated and randomly distributed in the inertial region. The most well-known predictions of the AEM are the logarithmic laws for streamwise or spanwise fluctuating velocity variances and the constant wall-normal fluctuating velocity variance. During the last decade, benefiting from the rapid development of advanced experimental and computational techniques, evidence supporting the AEM has been established

*hurf@lzu.edu.cn
†dswayb@126.com
‡rvinuesa@mech.kth.se

from experimental measurements [8–24], highly accurate numerical simulations [20,25–37], and reduced-order modeling [38–42]. Applications of AEM have arisen like generating turbulence inflow data [43]. Recent studies have also indicated that other types of eddies besides attached eddies coexist in the outer region of canonical wall turbulence [4,19,20,44–48].

Townsend [1] proposed the first AEM. He surmised that, in the inertial region of wall turbulence, predominant energy-containing eddies have diameters proportional to the distance of their centers from the wall, in a sense *attached* to the wall. He further assumed that turbulent flows are made up of contributions from attached eddies of various sizes with self-similar velocity distribution. Then the velocity covariance can be computed by summing up the contributions from all eddies with various sizes, which is

$$\langle u_i^+ u_j^+ \rangle(z) = \int_z^\delta p_e(h_e) I_{ij}(z/h_e) dh_e, \tag{1}$$

where $u_i^+ = u_i/U_\tau$, u_i is the fluctuating flow velocity in the ith direction, U_τ ($\equiv\sqrt{\tau_w/\rho}$, where τ_w is mean wall-shear stress and ρ is fluid density) is friction velocity, I_{ij} is the eddy intensity function which quantifies contribution by eddies of the same size, z is the wall-normal height from the wall, δ is the outer scale of a wall flow (boundary-layer thickness, pipe radius, or half-channel height), and $\langle\cdot\rangle$ indicates ensemble average. In this paper, x, y, and z denote coordinates in streamwise, spanwise, and wall-normal directions, respectively, and u, v, and w are the corresponding fluctuating velocities. Note that $p_e(h_e)$ denotes the probability density function (PDF) of a point located in an eddy with size h_e. Furthermore, Townsend deduced that for a small z/h_e, $I_{13} \propto z/h_e$. In order to reach a constant Reynolds shear stress $-\langle uw \rangle$, it is required that $p_e(h_e) \propto 1/h_e$ from Eq. (1). This is the well-known inverse law for p_e. Then, the logarithmic laws for streamwise and spanwise velocity variances and the constant law for wall-normal velocity variance can be obtained. In fact, Townsend did not invoke any representative eddies, and his theory was based on a continuous description of eddies, not a discrete one in three-dimensional space.

Perry and Chong [2] refined Townsend's AEM by introducing the Λ vortex as representative eddy. For a hierarchy of geometrically self-similar eddies whose size doubles with a factor of 2, together with the inverse PDF, i.e., $p_e(h_n) \propto 1/h_n$, Perry and Chong were able to obtain the same predictions of velocity covariances as those proposed by Townsend. To the authors' understanding, the AEM of Perry and Chong is a semidiscrete model, as they did not calculate three-dimensional flow fields via spatially distributed eddies, but utilized the eddy intensity function (or similar functions), and integrated it with the product of the eddy's PDF in a similar way as Townsend did, i.e., Eq. (1). The AEM of Perry and Chong was further improved in a series of works by Perry *et al.* [3], Perry and Marusic [4], and Marusic [5], e.g., extended from the wall region to the whole flow [3], extended to boundary layers with pressure gradient [4], as well as the adoption of the Π-vortex packet as representative eddy [5].

Woodcock and Marusic [6] improved the presentation of the AEM in a more rigorous way. They introduced the concept of population density of eddies in three-dimensional space (see their Appendix A). Let $M_e(h_n)$ be the number of eddies of scale n attached to the wall of a unit area, that is, the eddy's population density. By assuming that there are as many eddies of scale $n+1$ on an area of $(2L)^2$ as those of scale n on an area of L^2, they deduced that

$$M_e(h_n) \propto 2^{-2n}, \tag{2}$$

or

$$M_e(h_n)/M_e(h_1) = 2^{-2(n-1)} = (h_n/h_1)^{-2}, \tag{3}$$

where $h_n/h_1 = 2^{n-1}$. Equation (3) implies a -2 power law for the population density M_e with eddy size h_n. With the -2 power law for the eddy's population density, de Silva *et al.* [49] generated three-dimensional synthetic velocity fields by attached eddies for the first time, which is denoted as the fully discrete AEM. A packet of Λ vortices is chosen as representative eddy following the

hairpin-packet paradigm [50], which consists of seven Λ vortices with an average spacing of $0.4l$ (l is the wall-normal height of the largest eddy in the packet) and an inclination angle of 10°. The flow field was calculated according to the Biot-Savart law. This synthetic fully discrete AEM has been subsequently improved or applied in many aspects, e.g., generating wall-normal or spanwise velocity fields [51,52], accounting for the effect of spatial exclusion of eddies within the same scale [53], incorporating the meandering feature of large-scale structures to the flow direction [54], proposing a spectral-scaling-based extension of the AEM [55], and data-driven enhancement of the AEM [56]. Reasonable agreements between experimental measurements and synthetic realizations have been reported.

The hierarchical random and additive process (HRAP) formalism, proposed by Yang *et al.* [57–59], can be regarded as a simplified version of the AEM [7]. In this model, the (streamwise) velocity fluctuation induced by attached eddies is assumed to be an independent and identically distributed random variable. The same scaling laws for the streamwise, spanwise, and wall-normal velocity covariances with the AEM have be obtained. In addition, scaling laws for the moment-generating functions [57], two-point correlations [58], structure functions [60], and probability density [61] of turbulence velocity were also derived from the HRAP framework.

In the classical AEM, besides self-similar velocity distribution of attached eddies, another strong assumption is the eddy's probability density with size h_e following $p_e(h_e) \propto h_e^{-1}$, which was determined according to the constant Reynolds-shear-stress distribution robustly observed in numerous canonical wall-bounded turbulent flows. However, the constant Reynolds-shear-stress distribution may not hold in complex turbulent flows, hence neither does $p_e(h_e) \propto h_e^{-1}$. For example, many laboratory experiments and well-resolved simulations of adverse-pressure-gradient turbulent boundary layers (APGTBLs) have well-demonstrated nonconstant Reynolds-shear-stress distributions in the outer layer [62–69]. Therefore, an important question is whether attached eddies exist in complex turbulent flows. In this paper, we attempt to extend the classical AEM to general attached eddies with $p_e(h_e) \propto h_e^{-\alpha}$, where α is an arbitrary positive real number. It is expected that this generalization can be useful in deepening the understanding of one vital topic in turbulence research, i.e., the connection between coherent structures and turbulence statistics. Furthermore, we will connect the exponents of generalized power laws for the probability density, population density, area coverage, and volume fraction with the fractal dimension of general attached eddies, leading to a more complete knowledge of the attached eddies. It is noted that the terms eddies, motions, and coherent structures can be interchangeable in this paper [70,71].

The structure of the paper is as follows. In Sec. II, we will revisit the classical AEM and then extend it to the general attached eddies. In Sec. III, we will connect the power laws and the fractal dimension of the general attached eddies. The issue of the near-wall turbulence intensity peak scaling will be discussed in Sec. IV. The final conclusions will be given in Sec. V.

II. THEORY

A. The classical AEM

Here we give an overview of the classical Townsend's attached-eddy theory [1] and the HRAP formalism [57–59]. Wall-bounded turbulent flow is considered to be homogeneous in both streamwise and spanwise directions, as well as statistically stationary. The theory is mainly free of viscous effects, and thus is valid for $z^+ \gg 1$. The parallel velocity components, i.e., u and v, satisfy the free-slip condition. The wall-normal velocity obeys the impermeable condition. The attached eddies are assumed to be independently and randomly superimposed in the outer region for $z > z_r$, and shed footprints in the inner viscous region for $z < z_r$, where $z_r^+ = 100$ is the critical viscous cutoff height of inner and outer regions [72]. In the following, all variables are normalized by the viscous units, i.e., the friction velocity U_τ and kinematic viscosity ν, and the "+" superscript will be omitted (when it is not omitted, this is done for emphasis purposes).

1. Townsend's theory

Townsend [1] assumed that attached eddies have similar velocity distribution, as

$$\mathbf{u}(\mathbf{x}, \mathbf{x}_e) = \mathbf{f}\left(\frac{\mathbf{x} - \mathbf{x}_e}{h_e}\right), \tag{4}$$

where $\mathbf{x}_e = (x_e, y_e, h_e)$ is the center of a single eddy (h_e is eddy center height), and $\mathbf{u}$ is the induced velocity distribution of the eddy at $\mathbf{x}_e$.

Thus, the one-point velocity covariance contributed by two eddies at $\mathbf{x}_e$ and $\mathbf{x}'_e$ is

$$u_i(\mathbf{x}, \mathbf{x}_e)u_j(\mathbf{x}, \mathbf{x}'_e) = f_i\left(\frac{\mathbf{x} - \mathbf{x}_e}{h_e}\right)f_j\left(\frac{\mathbf{x} - \mathbf{x}'_e}{h'_e}\right). \tag{5}$$

The random distribution assumption of attached eddies implies that the velocity correlation from different eddies should be zero on average. Thus we only consider the nonzero velocity covariance contribution from one eddy, which is

$$u_i(\mathbf{x}, \mathbf{x}_e)u_j(\mathbf{x}, \mathbf{x}_e) = f_i\left(\frac{\mathbf{x} - \mathbf{x}_e}{h_e}\right)f_j\left(\frac{\mathbf{x} - \mathbf{x}_e}{h_e}\right). \tag{6}$$

The velocity covariance contributed by eddies with size h_e at a constant z plane ($z < h_e$) is

$$\langle u_i(z, h_e)u_j(z, h_e)\rangle = \iint \tilde{p}_e(\mathbf{x}_e)f_i\left(\frac{\mathbf{x} - \mathbf{x}_e}{h_e}\right)f_j\left(\frac{\mathbf{x} - \mathbf{x}_e}{h_e}\right)d\left(\frac{x_e}{h_e}\right)d\left(\frac{y_e}{h_e}\right), \tag{7}$$

where $\tilde{p}_e(\mathbf{x}_e)$ is the probability density of a point located in the eddy at $\mathbf{x}_e$, and should be independent of x_e and y_e, owing to the uniformly random distribution of eddies, satisfying

$$\tilde{p}_e(\mathbf{x}_e) = p_e(h_e), \tag{8}$$

where $p_e(h_e)$ is the probability density of a point located in eddies with size h_e. According to Eq. (7), we have

$$\langle u_i(z, h_e)u_j(z, h_e)\rangle = p_e(h_e)I_{ij}(z/h_e), \tag{9}$$

where

$$I_{ij}(z/h_e) = \iint f_i\left(\frac{\mathbf{x} - \mathbf{x}_e}{h_e}\right)f_j\left(\frac{\mathbf{x} - \mathbf{x}_e}{h_e}\right)d\left(\frac{x_e}{h_e}\right)d\left(\frac{y_e}{h_e}\right), \tag{10}$$

which is the eddy intensity function of Townsend [1]. The velocity covariance by all eddies is the summation or integral of eddies with size $h_e > z$ (smaller eddies do not contribute), resulting in Eq. (1).

At a constant z and letting $z^* = z/h_e$, we have $dz^*/z^* = -dh_e/h_e$ [73]. Therefore, Eq. (1) becomes

$$\langle u_i u_j\rangle(z) = \int_{z/\delta}^{1} h_e p_e(h_e) I_{ij}(z/h_e)\frac{dz^*}{z^*}. \tag{11}$$

Townsend [1] proposed the following asymptotic estimations for $z^* \to 0$:

$$I_{11} \to a_1, \quad I_{22} \to b_1, \quad I_{33} \to z^{*2}, \quad I_{13} \to z^*, \tag{12}$$

according to the velocity boundary conditions, with a_1 and b_1 being constants. By knowing $-\langle uw\rangle = 1$ in the inertial layer from numerous experimental measurements, it is deduced that $p_e(h_e) \propto h_e^{-1}$. Thus the scaling laws for the velocity covariances can be obtained using Eq. (12) as

$$\langle u^2\rangle = B_1 + A_1 \ln(\delta/z), \tag{13}$$

$$\langle v^2\rangle = B_2 + A_2 \ln(\delta/z), \tag{14}$$

$$\langle w^2\rangle = C_3, \tag{15}$$

where $A_1 \sim A_2$, $B_1 \sim B_2$, and C_3 are constants.

2. The HRAP formalism

The HRAP formalism [57–59] is regarded as a simplification of Townsend's theory [7]. In this model, the velocity or other quantity induced by the attached eddies is assumed to be an independent and identically distributed random variable.

In a discrete manner, the streamwise velocity fluctuation at z is expressed as

$$u^2 = \sum_{n=1}^{N} (p_e(h_n)\Delta h_n) a_n^2 \propto \sum_{n=1}^{N} a_n^2, \tag{16}$$

in which a_n^2 represents the contribution to u^2 by the attached eddies with size $h_n = \eta^{n-1} h_{\min}$ ($h_{\min} = z$ is the height of the smallest eddy felt at z, and $\eta = h_{n+1}/h_n$ is the successive constant size ratio of eddies), and $P_e(h_n) = p_e(h_n)\Delta h_n$ is the probability of a point located in the attached eddies with size h_n. Since $\Delta h_n = h_{n+1} - h_n = (\eta - 1)h_n$ and $p_e(h_n) \propto h_n^{-1}$, $P_e(h_n)$ is a constant and relation (16) holds.

The streamwise velocity variance can thus be obtained by

$$\langle u^2 \rangle \propto N \langle a^2 \rangle, \tag{17}$$

according to $\langle a_i a_j \rangle = \langle a^2 \rangle \delta_{ij}$ (note that a_i and a_j are identical and independent random variables if $i \neq j$), where δ_{ij} is the Kronecker symbol. The number of addends N is determined as follows. Since $h_{\max} = \eta^{N-1} h_{\min}$, we can get $N \approx \ln(h_{\max}/h_{\min})/\ln \eta$ when N is very large (which is true in high-Reynolds-number flows). As $h_{\max} \approx \delta$ and $h_{\min} = z$, it yields $N \approx \ln(\delta/z)/\ln \eta$. Substituting this relation into Eq. (17), one finally obtains

$$\langle u^2 \rangle \propto \langle a^2 \rangle \ln(\delta/z)/\ln \eta \propto \ln(\delta/z), \tag{18}$$

as $\langle a^2 \rangle$ and η are constants. Thus relation (18) can be written the same as relation (13). The scaling law for the spanwise-velocity variance (14) can be derived in a similar way.

For the wall-normal velocity fluctuation at z, the HRAP formalism gives [74]

$$w^2 = (p_e(h_1)\Delta h_1) C_w^2 a_1^2, \tag{19}$$

in which C_w is a constant. Equation (19) implies that the wall-normal velocity fluctuation is determined by the closest neighboring attached eddies at z. As a result, the wall-normal velocity variance is

$$\langle w^2 \rangle \propto \langle a^2 \rangle = \text{const}. \tag{20}$$

According to Eqs. (16) and (19), the Reynolds shear stress by attached eddies is

$$\langle uw \rangle \propto \langle a^2 \rangle = \text{const}. \tag{21}$$

The scaling predictions by the HRAP formalism, i.e., (18), (20), and (21), are exactly the same as those by Townsend's theory, thus they are consistent with each other for the classical attached eddies.

B. General attached eddies

Here we derive scaling laws for the velocity covariance of general attached eddies with $p_e(h_e) \propto h_e^{-\alpha}$ in the framework of both generalized Townsend's theory and the HRAP formalism.

1. Generalized Townsend's theory

First, we substitute $p_e(h_e) \propto h_e^{-\alpha}$ into Eq. (1), which yields

$$\langle u_i u_j \rangle \propto \int_z^\delta h_e^{-\alpha} I_{ij}(z/h_e) dh_e. \tag{22}$$

With the asymptotic relations (12), we can obtain

$$\langle u^2 \rangle \text{ and } \langle v^2 \rangle \propto \frac{1}{\alpha - 1}\left(\frac{1}{z^{\alpha-1}} - \frac{1}{\delta^{\alpha-1}}\right), \tag{23}$$

$$\langle w^2 \rangle \propto \frac{z^2}{\alpha + 1}\left(\frac{1}{z^{\alpha+1}} - \frac{1}{\delta^{\alpha+1}}\right), \tag{24}$$

$$\langle uw \rangle \propto \frac{z}{\alpha}\left(\frac{1}{z^{\alpha}} - \frac{1}{\delta^{\alpha}}\right). \tag{25}$$

Note that here we should exclude the case of $\alpha = 1$ to avoid singular scaling laws for $\langle u^2 \rangle$ and $\langle v^2 \rangle$, which should be obtained from the classical AEM. The cases of $\alpha = -1$ and 0 should also be excluded for nonsingular scaling laws for $\langle w^2 \rangle$ and $\langle uw \rangle$, respectively.

For the streamwise and spanwise velocity variance $\langle u^2 \rangle$ and $\langle v^2 \rangle$, as well as $z \ll \delta$ in the inertial layer, relation (23) can be reduced to

$$\begin{cases} \langle u^2 \rangle \text{ and } \langle v^2 \rangle \propto \dfrac{\delta^{1-\alpha}}{1-\alpha}\left[1 - \left(\dfrac{z}{\delta}\right)^{1-\alpha}\right] \propto \text{const}, & \text{if } \alpha < 1, \\ \langle u^2 \rangle \text{ and } \langle v^2 \rangle \propto \dfrac{z^{1-\alpha}}{\alpha-1}\left[1 - \left(\dfrac{z}{\delta}\right)^{\alpha-1}\right] \propto z^{1-\alpha}, & \text{if } \alpha > 1. \end{cases} \tag{26}$$

Thus the streamwise and spanwise velocity variances by general attached eddies are constants if $\alpha < 1$, and proportional to $z^{1-\alpha}$ if $\alpha > 1$.

For the wall-normal velocity variance $\langle w^2 \rangle$, as well as $z \ll \delta$ in the inertial layer, relation (24) can be reduced to

$$\begin{cases} \langle w^2 \rangle \propto -\dfrac{z^2\delta^{-(\alpha+1)}}{\alpha+1}\left[1 - \left(\dfrac{z}{\delta}\right)^{-(\alpha+1)}\right] \propto z^2, & \text{if } \alpha < -1, \\ \langle w^2 \rangle \propto \dfrac{z^{1-\alpha}}{\alpha+1}\left[1 - \left(\dfrac{z}{\delta}\right)^{\alpha+1}\right] \propto z^{1-\alpha}, & \text{if } \alpha > -1. \end{cases} \tag{27}$$

Thus the wall-normal velocity variance by general attached eddies is proportional to z^2 if $\alpha < -1$, and to $z^{1-\alpha}$ if $\alpha > -1$.

For the Reynolds shear stress $\langle uw \rangle$, as well as $z \ll \delta$ in the inertial layer, relation (25) can be reduced to

$$\begin{cases} \langle uw \rangle \propto -\dfrac{z\delta^{-\alpha}}{\alpha}\left[1 - \left(\dfrac{z}{\delta}\right)^{-\alpha}\right] \propto z, & \text{if } \alpha < 0, \\ \langle uw \rangle \propto \dfrac{z^{1-\alpha}}{\alpha}\left[1 - \left(\dfrac{z}{\delta}\right)^{\alpha}\right] \propto z^{1-\alpha}, & \text{if } \alpha > 0. \end{cases} \tag{28}$$

Thus the Reynolds shear stress by general attached eddies is proportional to z if $\alpha < 0$, and to $z^{1-\alpha}$ if $\alpha > 0$.

2. Generalized HRAP formalism

Next, we resort to generalizing the HRAP formalism.

For the streamwise velocity fluctuation, the relation $p_e(h_n) \propto h_n^{-\alpha}$ is substituted into Eq. (16), which yields

$$u^2 \propto \sum_{n=1}^{N} h_n^{1-\alpha} a_n^2. \tag{29}$$

Then the streamwise velocity variance is

$$\langle u^2 \rangle \propto \left(\sum_{n=1}^{N} h_n^{1-\alpha} \right) \langle a^2 \rangle. \tag{30}$$

With $h_n = \eta^{n-1} h_{\min} = \eta^{n-1} z$, we can get

$$\langle u^2 \rangle \propto \left(\sum_{n=1}^{N} q^{n-1} \right) z^{1-\alpha} \langle a^2 \rangle = \frac{1-q^N}{1-q} z^{1-\alpha} \langle a^2 \rangle, \tag{31}$$

where $q = \eta^{1-\alpha}$. In addition, since $N \approx \ln(\delta/z)/\ln \eta$, we can find

$$q^N \approx \left(\frac{\delta}{z} \right)^{(1-\alpha)}. \tag{32}$$

Note that if $\alpha < 1$, $q > 1$ since $\eta > 1$, and $q^N \gg 1$ when N is very large. Then Eq. (31) can be reduced to

$$\langle u^2 \rangle \propto q^N z^{1-\alpha} \propto \text{const}. \tag{33}$$

On the other hand, if $\alpha > 1$, $q < 1$ and $q^N \approx 0$ when N is very large. Therefore, Eq. (31) is simplified to

$$\langle u^2 \rangle \propto \frac{z^{1-\alpha}}{1-q} \langle a^2 \rangle \propto z^{1-\alpha}. \tag{34}$$

The HRAP modeling and resulting scaling laws for the spanwise velocity variance $\langle v^2 \rangle$ are similar to the streamwise one, so we do not repeat them here.

For the wall-normal velocity fluctuation, we substitute $p_e(h_n) \propto h_n^{-\alpha}$ into Eq. (19), and obtain

$$w^2 \propto h_1^{1-\alpha} a_1^2 = z^{1-\alpha} a_1^2. \tag{35}$$

Therefore, the wall-normal velocity variance satisfies

$$\langle w^2 \rangle \propto z^{1-\alpha}. \tag{36}$$

For the Reynolds shear stress, we can similarly get

$$\langle uw \rangle \propto z^{1-\alpha}. \tag{37}$$

It is clearly seen that the scaling laws for the streamwise and spanwise velocity variances by the generalized HRAP formalism, i.e., (33) and (34), are exactly the same as those by the generalized Townsend's theory, i.e., (26). The generalized HRAP prediction for the wall-normal velocity variance, i.e., (36), is the same as that by the generalized Townsend's theory with $\alpha > -1$, i.e., (27). In addition, the generalized HRAP prediction for the Reynolds shear stress, i.e., (37), is the same as that by the generalized Townsend's theory with $\alpha > 0$, i.e., (37). In the end, to make the generalized Townsend's theory and the generalized HRAP model consistent with each other, we speculate that $\alpha > 0$ should be enforced so that the exponent of the power law for the probability density p_e is negative.

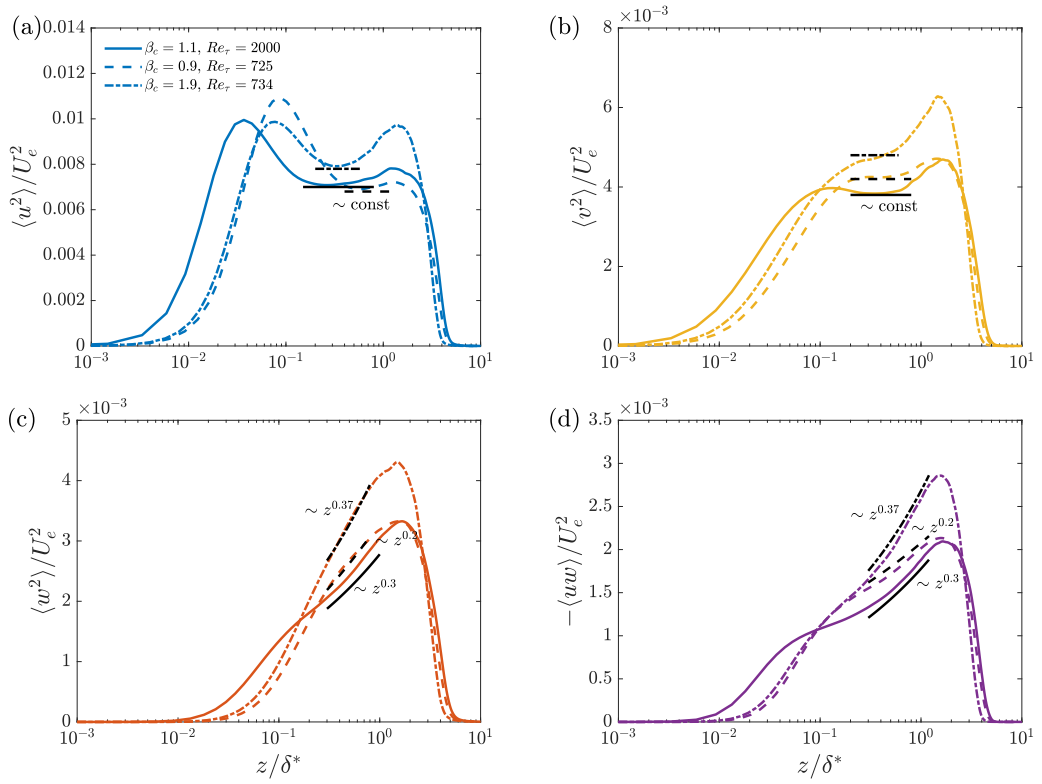

FIG. 1. Reynolds-stress profiles of adverse-pressure-gradient turbulent boundary layer flows with different Reynolds number Re_τ and the Clauser pressure-gradient parameter β_c from the high-fidelity simulation data of Pozuelo *et al.* [69] and Bobke *et al.* [66].

C. Evidence

We have revisited the classical Townsend's attached-eddy theory and the recent HRAP formalism. Then we extend both theories to the general attached eddies with probability density $p_e(h_e) \propto h_e^{-\alpha}$, where α can be an arbitrary positive real number. Scaling laws for the velocity covariances have been derived. Both theories yield consistent predictions. At the current stage, it is hoped that these theoretical predictions for the general attached eddies could be useful for elucidating the connection between coherent structures and turbulence statistics of complex turbulent flows. One possible case is adverse-pressure-gradient turbulent boundary layer flow. There has been extensive evidence showing that the magnitude of the Reynolds shear stress increases with the wall-normal distance in these flows [62–69,75], which may follow the scaling (37) with $0 < \alpha < 1$.

Figure 1 shows the Reynolds-stress profiles of various APGTBL flows with different friction Reynolds number Re_τ ($\mathrm{Re}_\tau = U_\tau\delta/\nu$) and Clauser pressure-gradient parameters β_c ($\beta_c = \delta^*/\tau_w dP/dx$, where δ^* is the displacement thickness and dP/dx is the mean streamwise pressure gradient) from the high-fidelity simulation data by Pozuelo *et al.* [69] and Bobke *et al.* [66]. It is seen that in the range of $\approx 0.2 < z/\delta^* <\approx 1.0$, the Reynolds-stress components display reasonable agreement with the scaling laws (26)–(28) by the generalized AEM with $0 < \alpha < 1$, i.e., $\langle u^2\rangle$ and $\langle v^2\rangle$ are almost constant, while $\langle w^2\rangle$ and $\langle uw\rangle$ follow $z^{1-\alpha}$. Moreover, according to Figs. 1(c) and 1(d), we find that the value of the exponent α monotonically decreases with the increase of the magnitude of the pressure-gradient parameter β_c. This is consistent with the fact that for very small β_c, it can be expected that the flow is closer to zero-pressure-gradient turbulent boundary layer (ZPGTBL) conditions, where the classical attached eddies with $\alpha = 1$ are observed. It should be

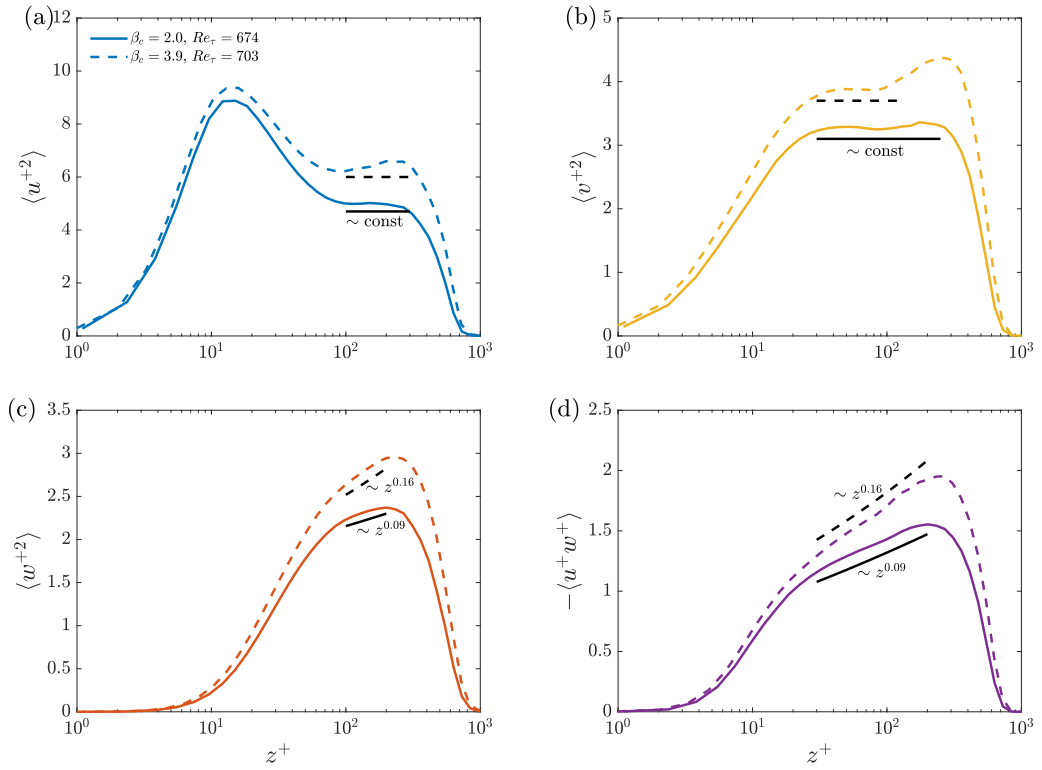

FIG. 2. Reynolds-stress profiles of turbulent NACA4412 wing boundary layer flow with different Reynolds number Re_τ and the Clauser pressure-gradient parameter β_c from the high-fidelity simulation data of Tanarro *et al.* [68].

noted that the present evidence shown in Fig. 1 is from APGTBL with mild streamwise pressure gradients. On the other hand, for APGTBL with a very strong pressure gradient ($\beta_c \to \infty$), the Reynolds stress may deviate from the proposed scalings [75]. This may be owing to the fact that the flow is more like a free shear layer than a ZPGTBL [75]. Therefore, it may be implausible that the attached eddies exist in this case. Also note that with a larger Reynolds number the inner and outer separation is more evident, and the wall-normal range within which the scaling laws are predicted by the generalized AEM is wider. This is consistent with the knowledge from the canonical wall-bounded turbulent flows, since the AEM is a theory more suitable for high-Reynolds-number flows.

Figure 2 displays the Reynolds-stress profiles of turbulent boundary layer flow over a NACA4412 wing at two streamwise locations with different values of the pressure-gradient parameter but with similar Reynolds numbers. It can be seen that the scaling laws given by the generalized AEM are also in good agreement with the wing data in the inertial region. In addition, as in APGTBL flows, the value of α fitted by the data decreases with the increase of β_c. The above results demonstrate that the present generalized AEM may predict reasonable Reynolds-stress scaling laws of different wall-bounded turbulent flows, including flat-plate APGTBLs and turbulent wings.

III. CASCADE SELF-SIMILARITY OF ATTACHED EDDIES

Although the classical attached-eddy model is very successful in predicting scaling laws in the inertial layer of canonical wall turbulence, several issues remain elusive. First, the connection of p_e with the eddy's spatial properties is unclear, e.g., the eddy's population density among others.

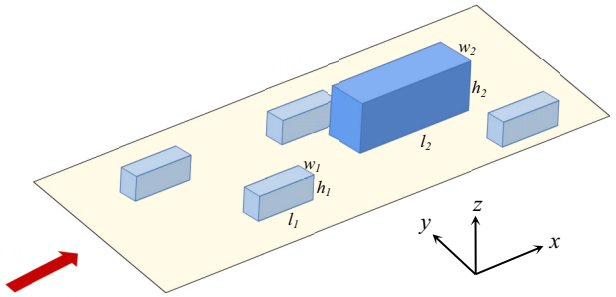

FIG. 3. Sketch of Townsend's wall-attached eddies with two hierarchies, where $h_2/h_1 = 2$. The geometry of an attached eddy with scale n is characterized by its height h_n, length l_n, and width w_n in three-dimensional space, respectively.

Perry and Chong [2] implicitly addressed this issue by assuming that the average spacing between eddies is proportional to the eddy's height and showed that such a hierarchy of wall-attached eddies corresponds to Townsend's AEM. However, this connection is indirect. Second, an empirical relation, $-\langle uw\rangle = 1$, was utilized to fix p_e in the AEM, which may be an unnecessary assumption.

In this section, we will directly connect the eddy's probability density with its population density, area coverage, and volume fraction, in a simple and clear way. It will be shown that the inverse law for p_e is equivalent to the -2 power law for the eddy's population density or constant area coverage. Therefore, the assumption of constant Reynolds-shear-stress distribution in the classical AEM is relieved, which in turn is also a prediction of the AEM. Furthermore, the power-law relationships of the classical attached eddies will be extended to the general attached eddies, and the exponents of the power laws will be connected with the fractal dimension of the general attached eddies.

A. The classical attached eddies

Figure 3 displays a sketch showing the attached eddies with two hierarchies for simplicity. Generally, the shape of the eddies is the same while their sizes vary according to their hierarchies, as illustrated in Fig. 3. We assume that the size of the eddies increases with a constant ratio η ($\eta = h_{n+1}/h_n$) according to the geometrical self-similarity, which requires that the lengths, widths, and heights of the eddies in different hierarchies are proportional to each other, as

$$\frac{h_2}{h_1} = \frac{l_2}{l_1} = \frac{w_2}{w_1} = \eta, \tag{38}$$

where (h_1, l_1, w_1) and (h_2, l_2, w_2) are the (height, length, width) of the first and second hierarchies of eddies, respectively, as shown in Fig. 3. We also implicitly assume that the sectional shape and size of the eddies are the same at each height. In Fig. 3, an attached eddy is represented by an elongated cube, just for illustration purposes.

Second, we assume that, for the classical attached eddies, the eddy's area coverage on a horizontal plane is independent of its size, resulting in the -2 power law for the eddy's population density. Let us take the two hierarchies of eddies illustrated in Fig. 3 as an example. The size of the small eddies is one-half of that of the large eddy in each direction, thus the number of small eddies should be four times larger to keep the same area coverage, for $\eta = 2$ illustrated in Fig. 3. Here constant area coverage means that the eddy's footprint fills the wall (or any other horizontal plane) with constant area fractions regardless of their sizes. With this picture in mind, we will derive the connection between the eddy's probability density and population density.

In probability theory, the probability density function $f(\xi)$ of a random variable ξ is defined by

$$f(\xi) = \frac{dF(\xi)}{d\xi}, \tag{39}$$

where $F(\xi)$ is the cumulative distribution function of ξ, and $F(\xi_0)$ represents the probability of $\xi < \xi_0$. In a discrete system, we can approximate Eq. (39) as

$$f(\xi_n) \approx \frac{\Delta F(\xi_n)}{\Delta \xi_n}, \tag{40}$$

where $\Delta F(\xi_n) = F(\xi_{n+1}) - F(\xi_n)$ is the probability at $\xi = \xi_n$, and $\Delta \xi_n = \xi_{n+1} - \xi_n$.

Now turn to Townsend's classical attached eddies. We aim to determine the eddy's probability density $p_e(h_n)$. Equation (40) now becomes

$$p_e(h_n) \approx \frac{\Delta F(h_n)}{\Delta h_n}, \tag{41}$$

where $F(h_n)$ is the cumulative distribution function of eddies with size h_n, and it represents the probability of $h < h_n$. Thus $\Delta F(h_n) = F(h_{n+1}) - F(h_n)$ is the probability of eddies with size h_n, or more precisely, the probability of a point located in the footprint of an eddy with size h_n, which is equivalent to the eddy area coverage $C_e(h_n)$. According to the constant coverage of the classical attached eddies, $\Delta F(h_n)$ is a constant. On the other hand, $\Delta h_n = h_{n+1} - h_n = (\eta - 1)h_n \propto h_n$. Therefore, we can easily obtain the inverse law for the eddy's probability density according to Eq. (41), i.e.,

$$p_e(h_n) \propto 1/h_n. \tag{42}$$

Note that this derivation is solely based on the assumptions of geometrical self-similarity and constant area coverage. No empirical assumption is invoked. Knowing the inverse law for the eddy's probability density, the predictions of velocity covariance by the AEM can be directly obtained, without prescribing the constant Reynolds-shear-stress distribution *a priori*. From a theoretical viewpoint, we relieve one unnecessary empirical assumption in the AEM. It can be further deduced that the volume fraction of the classical attached eddies follows a linear law, i.e., $V_e(h_n) \propto h_n$, as $V_e(h_n) \propto C_e(h_n)h_n$ (C_e is the eddy's area coverage). Here the volume fraction is defined as the ratio between the volume filled by attached eddies and the volume of total space.

A number of previous studies have reported a (or close to) -2 power law for the eddy's population density or the inverse law for the eddy's probability density by analyzing flow data. For example, Lozano-Durán *et al.* [76] showed a -2 power law for the population density of attached Reynolds-shear-stress clusters in turbulent channel flow. Cheng *et al.* [77] obtained a -1.9 power law for the population density of negative u eddies, a -1.6 power law for both negative and positive w eddies, and a -1.3 power law for positive u eddies in turbulent channel flows. Cheng *et al.* [78] further reported a -2.5 power law for the population density of negative streamwise wall shear stress fluctuations. Considering the probability density, de Silva *et al.* [79] observed an inverse law for the eddy's probability density of large-scale wall-coherent motions from two-dimensional particle-image-velocimetry data of turbulent boundary layers.

Recently, Hu *et al.* [80] were also able to observe close to -2 power laws for the eddy's population density of both positive and negative u and w clusters of attached eddies by analyzing flow data, using the spectral decomposition method of Hu *et al.* [20], the spectral linear stochastic estimation of Baars *et al.* [81], and the clustering methodology [76,77,82–86]. The flow data were extracted from the direct numerical simulation (DNS) of turbulent channel flow at $\mathrm{Re}_\tau = 5200$ [28], which is publicly available in Johns Hopkins Turbulence Database [87]. Here we give a brief overview of the extraction methodology. First, the flow velocity of all attached eddies was isolated by the spectral decomposition scheme of Hu *et al.* [20]. Second, the coherent velocity of that at the eddy's center z_c^+ ($z_c^+ = 100$, 200, 400, and 800, respectively) was calculated using the spectral linear stochastic estimation [81] with the reference height $z_r = z_c$. Third, the footprint velocity of

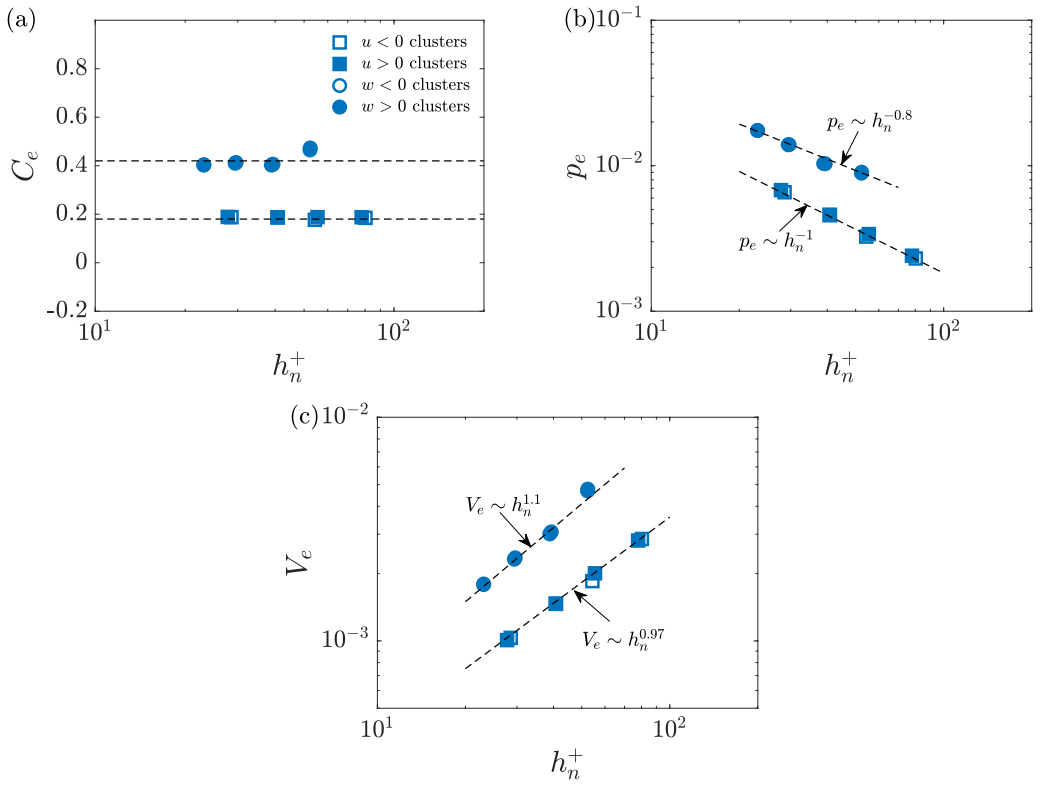

FIG. 4. (a) Area coverage, (b) probability density, and (c) volume fraction of discrete hierarchies of Townsend's wall-attached eddies varying with the eddy's height, extracted from turbulent channel flow at $\mathrm{Re}_\tau = 5200$ [28].

each hierarchy of attached eddies was obtained by subtracting the footprint velocity of larger eddies from the coherent velocity in a top-down manner. Last, the clustering methodology [76,77,82–86] was adopted to analyze the geometrical and population properties of each hierarchy of attached eddies. The clustering percolation parameter α_c is set to 1.3, as it has been shown that the results are not sensitive to it [80].

We further examine whether the probability density, area coverage, and volume fraction of the extracted eddies by Hu *et al.* [80] follow the inverse law, constant law, and linear law, respectively. The average size of each hierarchy of eddies is denoted by l_n, w_n, and h_n in length, width, and height, respectively, which are determined by the size of the bounding box enclosing an eddy cluster. Let $N_{e,n}$ be the total number of the extracted eddy clusters of the nth hierarchy. The eddy area coverage can be calculated as $C_e(h_n) = N_{e,n} l_n w_n/(N_f L_x L_y)$, where N_f is the total number of flow-field snapshots used in the calculation, while L_x and L_y are the lengths of the computational domain in x and y, respectively. The eddy's probability density is determined by $p_e(h_n) = C_e(h_n)/h_n$, according to Eq. (41). The eddy's volume fraction is obtained by $V_e(h_n) = N_{e,n} l_n w_n h_n/(N_f L_x L_y L_z)$, where L_z is the height of the simulation domain. The results are shown in Fig. 4. It can be observed that for both positive and negative u and w clusters, the eddy's area coverage C_e approximately follows a constant law, the eddy's probability density p_e approximately follows a -1 power law, and the eddy's volume fraction satisfies a linear law, in good agreement with the theoretical argument. It should be noted that the viscous-scaled eddy's height h_n^+ appears to be relatively small ($10 < h_n^+ < 100$). This is because only intense velocity fluctuations are included in the clustering analysis, therefore their sizes are much smaller than the eddy's center height [80]. Despite this, the extracted velocity footprints

at each height do have coherence with those at the center height, which deeply penetrate into the near-wall region, benefiting from the usage of the spectral linear stochastic estimation method [81]. We also note that it may be interesting to use more advanced methods involving nonlinearities like deep neural networks [88] to estimate the footprints.

B. The general attached eddies

In this subsection, we connect the exponents of the power laws for the probability density, population density, area coverage, and volume fraction with the fractal dimension of the general attached eddies.

The generalized power laws for the probability density and population density of eddies with size h_n are

$$p_e(h_n) \propto h_n^{-\alpha}, \quad M_e(h_n) \propto h_n^{-\beta}, \tag{43}$$

where α and β are arbitrary real numbers. According to the geometrical definitions, the eddy's area coverage C_e and volume fraction V_e follow

$$C_e(h_n) \propto M_e(h_n) h_n^2 \propto h_n^{2-\beta} = h_n^{-\gamma}, \tag{44}$$

$$V_e(h_n) \propto C_e(h_n) h_n \propto h_n^{3-\beta} = h_n^{1-\gamma} = h^{-\zeta}. \tag{45}$$

We resort to Eq. (41) to obtain

$$p_e(h_n) = \frac{\Delta F(h_n)}{\Delta h_n} \propto \frac{C_e(h_n)}{\Delta h_n} \propto h_n^{1-\beta}. \tag{46}$$

From the above derivations, we can directly relate the exponents of the generalized power laws for the probability density (α), population density (β), area coverage (γ), and volume fraction (ζ) with each other, as

$$\beta = \alpha + 1, \quad \gamma = \alpha - 1, \quad \zeta = \alpha - 2. \tag{47}$$

Therefore, for the general self-similar attached eddies, the power-law exponents α, β, γ, and ζ are dependent on each other. In other words, if we obtain any one of them, the other three can be directly determined from the relations (47).

In the context of fractality, self-similarity indicates a fractal invariant under ordinary geometric similarity; to quote Mandelbrot, "when each piece of a shape is geometrically similar to the whole, both the shape and the cascade that generates it are called self-similar" [89]. Thus, general self-similarity indicates both geometrical and cascade self-similarities. The geometrical self-similarity of attached eddies is well depicted in Fig. 3 and Eq. (38). On the other hand, the classical attached eddies with $\beta = 2$ constitute a good example for the cascade self-similarity, like the perfect-binary-tree-like structure illustrated in Perry and Chong [2] and Woodcock and Marusic [6]. Nonetheless, any cascade with a constant β can be self-similar in general, as any perfect tree structure is self-similar. Thus, we can imagine that the general attached eddies are fractal-like objects. Next, we will connect the exponents α, β, γ, and ζ with the fractal dimension D_e of the general self-similar attached eddies.

Interestingly, fractals can be manifested by power laws for surface area or volume with scale [89], which in our case can be expressed as

$$C_e(h_n) \propto h_n^{2-D_e}, \tag{48}$$

or

$$V_e(h_n) \propto h_n^{3-D_e}. \tag{49}$$

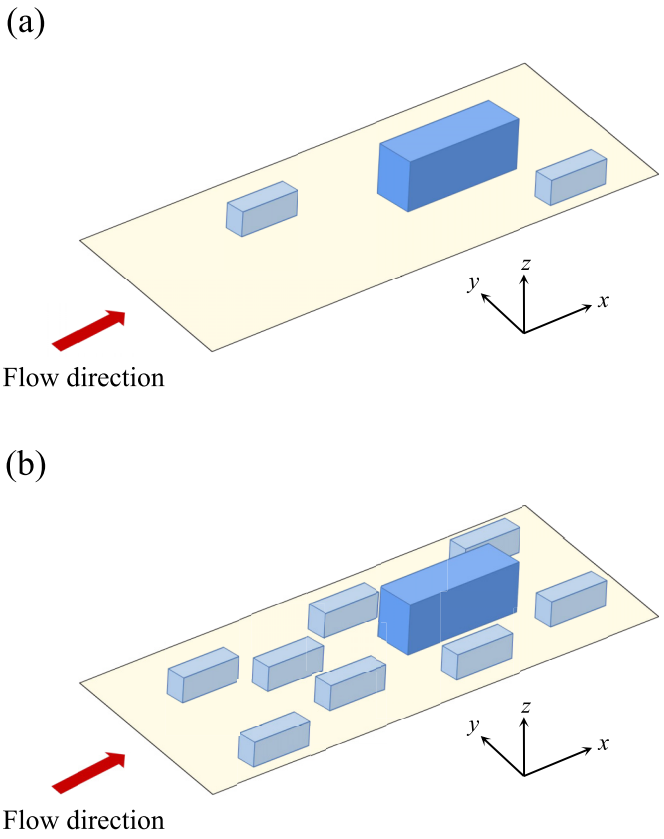

FIG. 5. Sketch of self-similar wall-attached eddies with two hierarchies and $h_2/h_1 = 2$: (a) $\beta = 1$ and (b) $\beta = 3$.

By comparing (48) or (49) with (44) or (45), we can simply find

$$D_e = \alpha + 1 = \beta = \gamma + 2 = \zeta + 3. \tag{50}$$

Relation (50) indicates that the exponent of the generalized power law for the eddy's population density is equivalent to the eddy's fractal dimension. For Townsend's classical attached eddies, we already know that $\alpha = 1$, hence $D_e = 2$ according to (50). For the footprints of eddies on a surface, $D_e = 2$ implies that the eddy's fractal dimension is the same as the two-dimensional topological dimension, thus they are space filling, while in three-dimensional space the fractal dimension is smaller than the topological dimension, thus non-space-filling [90,91]. It is also noted that Lozano-Durán *et al.* [76] also estimated the fractal dimension of Reynolds-shear-stress clusters as 2, the same as that of classical Townsend's attached eddies.

We illustrate two other scenarios of general self-similar attached eddies with $\beta = 1$ and 3, respectively, as shown in Fig. 5. Assuming $h_2/h_1 = 2$, the number of the first-hierarchy eddies is two times that of the second-hierarchy eddies with $\beta = 1$, and eight times with $\beta = 3$. According to (47), the probability density follows $p_e(h_n) \propto$ const and h_n^{-2}, the area coverage obeys $C_e(h_n) \propto h_n$ and h_n^{-1}, and the volume fraction complies $V_e(h_n) \propto h_n^2$ and const, respectively. This illustration emphasizes that Townsend's classical attached eddies, which fit well in canonical turbulence, are only one of many possibilities of general self-similar eddies. We may not exclude other possibilities of the existence of eddy organization. It should be noted that $\beta = 1$ implies $\alpha = 0$, which leads

to a singular scaling law for the Reynolds shear stress, i.e., Eq. (28). Therefore, Fig. 5 is only for illustration purposes.

IV. DISCUSSION ON THE SCALING OF THE NEAR-WALL STREAMWISE TURBULENCE INTENSITY PEAK

Scaling of the near-wall peak of the streamwise turbulence intensity has recently attracted extensive attention [92–96]. A wider range of studies suggests that the traditional viscous scaling fails for the near-wall turbulence intensity, which increases with the Reynolds number. This is mostly attributed to the growing influence of outer large-scale and very-large-scale motions on the near-wall region [97]. However, there exists controversy on how the near-wall peak grows with the Reynolds number, and whether its infinite asymptotic value is bounded. For example, if the scaling law for $\langle u^2\rangle$ given by the AEM, i.e., Eq. (13), is simply extrapolated to $y^+ = 15$ where the maximum streamwise turbulence intensity is located, one can also obtain a logarithmic law for $\langle u^2\rangle_{\max}$ with Re_τ [98], i.e., $\langle u^2\rangle_{\max} = B + A\ln Re_\tau$ (A and B are constants). In this case, it is obvious that $\langle u^2\rangle_{\max}$ is unbounded if $\mathrm{Re}_\tau \to \infty$. Note that here A is much smaller than A_1, and it is found that $A \approx A_1/2$ from empirical data [92]. On the other hand, Skouloudis and Hwang [95] found that $\langle u^2\rangle_{\max}$ follows $A_\infty - B_\infty/\ln \mathrm{Re}_\tau$ (A_∞ and B_∞ are constants) by a resolvent-based reduced-order model with quasilinear approximation. Particularly, Chen and Sreenivasan [93] proposed that $\langle u^2\rangle_{\max}(\infty) - \langle u^2\rangle_{\max}(\mathrm{Re}_\tau) \propto \mathrm{Re}_\tau^{-1/4}$ according to bounded wall dissipation rate, thus $\langle u^2\rangle_{\max}$ is bounded with $\mathrm{Re}_\tau \to \infty$.

Here we try to inspect this issue from the viewpoint of coherent structures closely related to attached eddies. According to the inner-outer decomposition [72,81,99,100], the near-wall ($y^+ < 100$) streamwise velocity fluctuation can be decomposed as

$$u = u_i + u_o = u_i + \underbrace{u_s + u_a + u_d}_{\text{outer footprints}}, \tag{51}$$

where u_i is the velocity fluctuation of the inner motions or the so-called near-wall cycle [101–103], which is believed to be Reynolds-number invariant; u_s is the footprint velocity of outer small-scale eddies; u_a is the footprint velocity of attached eddies; and u_d is the footprint velocity of very-large-scale detached eddies [20]. Since the different velocity components are assumed to be independent of each other, one can obtain

$$\langle u^2\rangle = \langle u_i^2\rangle + \langle u_o^2\rangle = \langle u_i^2\rangle + \langle u_s^2\rangle + \langle u_a^2\rangle + \langle u_d^2\rangle. \tag{52}$$

According to the spectral linear stochastic estimation of near-wall footprints of outer motions [72,81], we have

$$u_s = F_x^{-1}[\widehat{H}\widehat{u}_s(y_o^+)], \quad u_a = F_x^{-1}[\widehat{H}\widehat{u}_a(y_o^+)], \quad u_d = F_x^{-1}[\widehat{H}\widehat{u}_d(y_o^+)], \tag{53}$$

$$\widehat{H} = \frac{\langle \widehat{u}(y^+)\widehat{u}^*(y_o^+)\rangle}{\langle \widehat{u}(y_o^+)\widehat{u}^*(y_o^+)\rangle}, \tag{54}$$

where F_x^{-1} is the inverse Fourier transform in the streamwise direction, the hat indicates quantity after streamwise Fourier transform, the star symbol indicates complex conjugate, $\widehat{H}$ is the complex kernel function of the spectral linear stochastic estimation [81], $y_o^+ = 100$ is the reference height for calculating near-wall outer footprints [72], and the definitions of $\widehat{u}_s$, $\widehat{u}_a$, and $\widehat{u}_d$ in the outer region are

$$\widehat{u}_s = \begin{cases} \widehat{u}, & \lambda_x^+ < y^+/\tan\theta, \\ 0, & \text{otherwise}, \end{cases} \tag{55}$$

$$\widehat{u}_a = \begin{cases} \widehat{u}, & y^+/\tan\theta < \lambda_x^+ < \beta_a\delta^+, \\ 0, & \text{otherwise}, \end{cases} \tag{56}$$

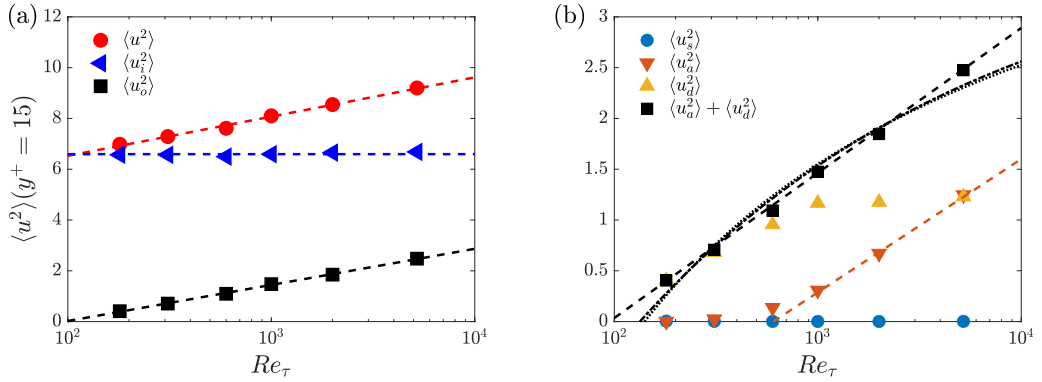

FIG. 6. Decomposition of the peak streamwise turbulence intensity $\langle u^2 \rangle$ at $y^+ = 15$ from DNS data of channel flows [28,72,104]. (a) Comparison of $\langle u^2 \rangle$, $\langle u_i^2 \rangle$, and $\langle u_o^2 \rangle$. Red dashed line, $\langle u^2 \rangle = 0.67 \ln \mathrm{Re}_\tau + 3.44$; blue dashed line, $\langle u_i^2 \rangle = 6.59$; black dashed line, $\langle u_o^2 \rangle = 0.62 \ln \mathrm{Re}_\tau - 2.82$. (b) Comparison of $\langle u_s^2 \rangle$, $\langle u_a^2 \rangle$, and $\langle u_d^2 \rangle$. Black dashed line, $\langle u_a^2 \rangle + \langle u_d^2 \rangle = 0.62 \ln \mathrm{Re}_\tau - 2.83$; black dashed-dotted line, $\langle u_a^2 \rangle + \langle u_d^2 \rangle = 3.88 - 13.19 \mathrm{Re}_\tau^{-1/4}$; black dotted line, $\langle u_a^2 \rangle + \langle u_d^2 \rangle = 5.46 - 27.01/\ln \mathrm{Re}_\tau$; red dashed-dotted line, $\langle u_a^2 \rangle = 0.57 \ln \mathrm{Re}_\tau - 3.65$.

and

$$\widehat{u}_d = \begin{cases} \widehat{u}, & \lambda_x^+ > \beta_a \delta^+, \\ 0, & \text{otherwise.} \end{cases} \tag{57}$$

Here, λ_x is the streamwise wavelength, $\theta = 10^\circ$, and $\beta_a = 4$ for channel flow [20]. It should be noted that attached eddies are statistical structures [7]. The characteristics of the attached eddies displayed here are all statistical measures that were obtained by averaging over plenty of flow-field realizations.

Figure 6 displays the Reynolds-number dependence of the decomposed streamwise turbulence intensities at $y^+ = 15$, according to Eq. (52). The utilized datasets are from DNS of turbulent channel flows [28,72,104]. There are several relevant observations that can be made from Fig. 6.

(i) The magnitude of $\langle u_i^2 \rangle$ at $y^+ = 15$ is almost Reynolds-number invariant and constitutes more than 70% of the total intensity $\langle u^2 \rangle$ in the range of Reynolds number shown here. The magnitude of $\langle u_o^2 \rangle$ at $y^+ = 15$ increases with Reynolds number, approximately following $0.62 \ln \mathrm{Re}_\tau - 2.82$.

(ii) The magnitude of $\langle u_s^2 \rangle$ at $y^+ = 15$ is very small and can be neglected compared with the other components. The magnitude of $\langle u_a^2 \rangle + \langle u_d^2 \rangle$ at $y^+ = 15$ increases with Reynolds number in a logarithmic form approximately, which is well fitted by $0.62 \ln \mathrm{Re}_\tau - 2.83$. The slope 0.62 is very close to that by fitting the total $\langle u^2 \rangle_{\max}$ [28,92], indicating that the logarithmic increase of $\langle u^2 \rangle_{\max}$ with Re_τ is mostly from outer footprints. In addition, best fits for the $\mathrm{Re}_\tau^{-1/4}$ and $1/\ln \mathrm{Re}_\tau$ deficit laws are also included for comparison.

(iii) By extrapolating the data to low Reynolds numbers, it can be found that $\langle u_o^2 \rangle \approx 0$ with $\mathrm{Re}_\tau \approx 100$, thus the outer-footprint intensity vanishes at this Reynolds number. This is consistent with and confirms that $\mathrm{Re}_\tau \approx 100$ is the critical Reynolds number where outer motions emerge [105]. It can also be informed from the analysis of wall-shear stress fluctuations [106].

(iv) Both $\langle u_a^2 \rangle$ and $\langle u_d^2 \rangle$ increase with the Reynolds number, but their variations are quite different. A major commonality is that their own variation significantly changes at $\mathrm{Re}_\tau = 1000$. At $\mathrm{Re}_\tau < 1000$, $\langle u_a^2 \rangle$ slowly increases while $\langle u_d^2 \rangle$ rapidly increases with Re_τ. At $\mathrm{Re}_\tau > 1000$, $\langle u_a^2 \rangle$ increases much more rapidly in a logarithmic manner approximately, i.e., $0.57 \ln \mathrm{Re}_\tau - 3.65$, while $\langle u_d^2 \rangle$ varies with a weak Re_τ dependence. Thus, $\mathrm{Re}_\tau = 1000$ can be regarded as the critical Reynolds number where the variations of $\langle u_a^2 \rangle$ and $\langle u_d^2 \rangle$ with Re_τ substantially change. The weak

Re_τ dependence of $\langle u_d^2 \rangle$ can also be inferred from Fig. 12 of Hu *et al.* [20], in which it can be observed that $\langle u_d^2 \rangle$ at $y^+ = 100$ is almost invariant with Re_τ at high Reynolds numbers.

Therefore, the present analysis of channel flow DNS data supports the logarithmic increase of $\langle u^2 \rangle_{\max}$ with Re_τ in the range of $\mathrm{Re}_\tau = 180$–5200. The origin of the logarithmic increase is solely from the outer footprints. We have identified different contributions and behaviors of attached eddies and very-large-scale detached eddies and determined $\mathrm{Re}_\tau = 1000$ as the critical Reynolds number for their Reynolds-number dependence. We would like to stress that this conclusion is based on a relatively narrow Reynolds-number range, and no definitive statement can be made regarding the scaling and the Re_τ trend in the asymptotic regime. The $\mathrm{Re}_\tau^{-1/4}$ deficit law [93,94] or the $1/\ln \mathrm{Re}_\tau$ law [95] may very well be the correct representation at much higher Reynolds number, as discussed next. One possibility is if $\langle u_a^2 \rangle$ keeps the logarithmic growth for $\mathrm{Re}_\tau > 1000$ as the AEM predicts, then it would be required that $\langle u_d^2 \rangle$ gradually decreases at large Re_τ. The other possibility is if $\langle u_d^2 \rangle$ keeps the current weak Re_τ dependence for $\mathrm{Re}_\tau > 1000$, one would expect that $\langle u_a^2 \rangle$ deviates from the logarithmic increase by the AEM prediction at large Re_τ. To verify the two possibilities, high-quality data from DNS and experimental measurements at much higher Reynolds numbers are very much needed. Last, if we extrapolate the generalized scaling laws for $\langle u_a^2 \rangle$ to the near-wall region, i.e., (33) and (34), it is inferred that $\langle u_a^2 \rangle_{\max} \propto \text{const}$ with $0 < \alpha < 1$, or $\langle u_a^2 \rangle_{\max} \propto z_{\max}^{1-\alpha}$ with $\alpha > 1$. However, in complex turbulent flows, we know little about the scalings for $\langle u_i^2 \rangle$ and $\langle u_d^2 \rangle$, hence no definite statement regarding near-wall $\langle u^2 \rangle_{\max}$ can be made at the current stage.

V. CONCLUDING REMARKS

In the present paper, we extend the attached-eddy model to general attached eddies with the eddy's probability density obeying $p_e(h_e) \propto h_e^{-\alpha}$, where α is an arbitrary positive real number. Scaling laws for velocity covariance (Reynolds stress) are obtained as follows:

$$\begin{cases} \langle u^2 \rangle \propto \text{const},\ \langle v^2 \rangle \propto \text{const},\ \langle w^2 \rangle \propto z^{1-\alpha},\ \langle uw \rangle \propto z^{1-\alpha}, & \text{if } 0 < \alpha < 1, \\ \langle u^2 \rangle \propto z^{1-\alpha},\ \langle v^2 \rangle \propto z^{1-\alpha},\ \langle w^2 \rangle \propto z^{1-\alpha},\ \langle uw \rangle \propto z^{1-\alpha}, & \text{if } \alpha > 1. \end{cases} \tag{58}$$

We expect that these scaling laws and the existence of the general attached eddies can be confirmed in complex wall turbulent flows. Preliminary evidence for the validity of the model from high-fidelity simulations of adverse-pressure-gradient turbulent boundary layers [66,69] and turbulent wing flow [68] is provided, in which all the Reynolds-stress components well follow the above scaling laws in the inertial layer with $0 < \alpha < 1$.

The cascade self-similarity of attached eddies is manifested by power laws for the probability density, population density, area coverage, and volume fraction of eddies. We directly connect the exponents of these power laws with the fractal dimension of the general attached eddies in a simple and clear way. Empirical evidence from the extraction results of Hu *et al.* [80] supports the present theoretical argument for the classical attached eddies. In addition, it is revealed that the fractal dimension of the general attached eddies is the same as the exponent of the power law for the eddy's population density. Therefore, we highlight that the scaling laws of turbulence statistics in the inertial layer of wall-bounded turbulent flows can be directly linked to the characteristics of the cascade self-similarity of general attached eddies. We believe that the scaling laws derived here and the generalized power-law relationships can be useful to provide a deeper understanding of the connection between coherent structures and turbulence statistics, and that they can also be useful diagnostic tools for the cascade self-similarity of eddies in complex wall-bounded turbulent flows.

Furthermore, we have demonstrated that the inverse law for eddy probability density is equivalent to the -2 power law for population density, which in fact implies a particular cascade self-similarity of the classical Townsend's attached eddies. Thus there is no need to assume a constant Reynolds-shear-stress distribution *a priori*, which in turn is also a prediction of the AEM. In fact, in the framework of the AEM, the inverse law for the probability density or the -2 power law for the population density can yield the constant Reynolds-shear-stress distribution, and vice versa.

Therefore, mathematically they are equivalent. However, from a physical point of view, structures are more likely the cause and statistics are the effects. With this causality consideration, we believe that the constant Reynolds-shear-stress distribution is a result of such an arrangement of attached eddies.

Finally, we inspect the Reynolds-number dependence of the near-wall streamwise peak turbulence intensity in the context of attached eddies and inner-outer decomposition. The present analysis principally supports the logarithmic increase of $\langle u^2 \rangle_{\max}$ with Re_τ in the narrow range of Reynolds number of the analyzed data. The logarithmic law is predominantly associated with the footprints of the attached eddies and the very-large-scale detached eddies. The quantitative contributions and statistical behaviors of the attached eddies and very-large-scale detached eddies with Re_τ are quite different. At $\mathrm{Re}_\tau > 1000$, the contribution by the attached eddies follows a logarithmic increase with Re_τ, while that of the very-large-scale detached eddies exhibits a very weak Re_τ dependence. However, two possibilities for the existence of alternative laws are also discussed, and the need for high-fidelity data at high Reynolds numbers is emphasized.

For future studies, we have several considerations. First, scaling laws for other turbulence statistics by the general attached eddies can be derived, such as high-order moments [98,107], moment-generating functions [57], structure functions [60,108–110], and two-point correlations [58,73]. Second, direct evidence for the power laws of the population density, probability density, area coverage, and volume fraction of the general attached eddies is desired, similar to Fig. 4 for the classical attached eddies. This requires a decomposition of the general attached eddies and outer very-large-scale motions first, like what has been done in the canonical turbulent flows [20,80]. Third, evidence from other types of flows is also needed, besides the APGTBL and wing flows presented in this paper.

ACKNOWLEDGMENTS

R.H. acknowledges financial support from the National Natural Science Foundation of China (Grants No. 11972175 and No. 92052202). S.D. acknowledges financial support from the National Natural Science Foundation of China (Grant No. 12072306). R.V. acknowledges financial support from the Swedish Research Council. The authors sincerely thank Jingxuan Zhang for providing the data shown in Fig. 6; Le Fang for pointing out mistakes in the derivation of (24) and (25); Xiang Yang, Cheng Cheng, Jie Yao, and Weipeng Li for useful suggestions; as well as the anonymous reviewers for valuable comments that helped to significantly improve the quality of the paper.

The authors report no conflict of interest.

[1] A. Townsend, *The Structure of Turbulent Shear Flow* (Cambridge University, New York, 1976).

[2] A. E. Perry and M. S. Chong, On the mechanism of wall turbulence, J. Fluid Mech. **119**, 173 (1982).

[3] A. E. Perry, S. Henbest, and M. S. Chong, A theoretical and experimental study of wall turbulence, J. Fluid Mech. **165**, 163 (1986).

[4] A. E. Perry and I. Marusic, A wall-wake model for the turbulence structure of boundary layers. Part 1. Extension of the attached eddy hypothesis, J. Fluid Mech. **298**, 361 (1995).

[5] I. Marusic, On the role of large-scale structures in wall turbulence, Phys. Fluids **13**, 735 (2001).

[6] J. D. Woodcock and I. Marusic, The statistical behaviour of attached eddies, Phys. Fluids **27**, 015104 (2015).

[7] I. Marusic and J. P. Monty, Attached eddy model of wall turbulence, Annu. Rev. Fluid Mech. **51**, 49 (2019).

[8] J. F. Morrison, B. J. McKeon, W. Jiang, and A. J. Smits, Scaling of the streamwise velocity component in turbulent pipe flow, J. Fluid Mech. **508**, 99 (1999).

[9] M. Hultmark, M. Vallikivi, S. C. C. Bailey, and A. J. Smits, Turbulent Pipe Flow at Extreme Reynolds Numbers, Phys. Rev. Lett. **108**, 094501 (2012).

[10] I. Marusic, J. P. Monty, M. Hultmark, and A. J. Smits, On the logarithmic region in wall turbulence, J. Fluid Mech. **716**, R3 (2013).
[11] P. Vincenti, J. Klewicki, C. Morrill-Winter, C. M. White, and M. Wosnik, Streamwise velocity statistics in turbulent boundary layers that spatially develop to high Reynolds number, Exp. Fluids **54**, 1629 (2013).
[12] M. Vallikivi, M. Hultmark, and A. J. Smits, Turbulent boundary layer statistics at very high Reynolds number, J. Fluid Mech. **779**, 371 (2015).
[13] L. H. O. Hellström, I. Marusic, and A. J. Smits, Self-similarity of the large-scale motions in turbulent pipe flow, J. Fluid Mech. **792**, R1 (2016).
[14] W. J. Baars, N. Hutchins, and I. Marusic, Self-similarity of wall-attached turbulence in boundary layers, J. Fluid Mech. **823**, R2 (2017).
[15] R. Örlü, T. Fiorini, A. Segalini, G. Bellani, A. Talamelli, and P. H. Alfredsson, Reynolds stress scaling in pipe flow turbulence-first results from CICLoPE, Phil. Trans. R. Soc. A **375**, 20160187 (2017).
[16] M. Heisel, T. Dasari, Y. Liu, J. Hong, F. Coletti, and M. Guala, The spatial structure of the logarithmic region in very-high-Reynolds-number rough wall turbulent boundary layers, J. Fluid Mech. **857**, 704 (2018).
[17] M. Samie, I. Marusic, N. Hutchins, M. K. Fu, Y. Fan, M. Hultmark, and A. J. Smits, Fully resolved measurements of turbulent boundary layer flows up to $Re_\tau = 20\,000$, J. Fluid Mech. **851**, 391 (2018).
[18] D. Krug, W. J. Baars, N. Hutchins, and I. Marusic, Vertical coherence of turbulence in the atmospheric surface layer: Connecting the hypotheses of Townsend and Davenport, Boundary-Layer Meteorol. **172**, 199 (2019).
[19] W. J. Baars and I. Marusic, Data-driven decomposition of the streamwise turbulence kinetic energy in boundary layers. Part 2. Integrated energy and A_1, J. Fluid Mech. **882**, A26 (2020).
[20] R. Hu, X. I. A. Yang, and X. Zheng, Wall-attached and wall-detached eddies in wall-bounded turbulent flows, J. Fluid Mech. **885**, A30 (2020).
[21] R. Deshpande, J. P. Monty, and I. Marusic, Active and inactive components of the streamwise velocity in wall-bounded turbulence, J. Fluid Mech. **914**, A5 (2021).
[22] X. Li, G. Wang, and X. Zheng, Logarithmic energy profile of the streamwise velocity for wall-attached eddies along the spanwise direction in turbulent boundary layer, Phys. Fluids **33**, 105119 (2021).
[23] L.-W. Wang, C. Pan, and J.-J. Wang, Wall-attached and wall-detached eddies in proper orthogonal decomposition modes of a turbulent channel flow, Phys. Fluids **34**, 095124 (2022).
[24] M. Puccioni, M. Calaf, E. R. Pardyjak, S. Hoch, T. J. Morrison, A. Perelet, and G. V. Iungo, Identification of the energy contributions associated with wall-attached eddies and very-large-scale motions in the near-neutral atmospheric surface layer through wind LiDAR measurements, J. Fluid Mech. **955**, A39 (2023).
[25] J. Jiménez and S. Hoyas, Turbulent fluctuations above the buffer layer of wall-bounded flows, J. Fluid Mech. **611**, 215 (2008).
[26] J. A. Sillero, J. Jiménez, and R. D. Moser, One-point statistics for turbulent wall-bounded flows at Reynolds numbers up to $\delta^+ \approx 2000$, Phys. Fluids **25**, 105102 (2013).
[27] M. Bernardini, S. Pirozzoli, and P. Orlandi, Velocity statistics in turbulent channel flow up to $Re_\tau = 4000$, J. Fluid Mech. **742**, 171 (2014).
[28] M. K. Lee and R. D. Moser, Direct numerical simulation of turbulent channel flow up to $Re_\tau \approx 5200$, J. Fluid Mech. **774**, 395 (2015).
[29] L. Agostini and M. Leschziner, Spectral analysis of near-wall turbulence in channel flow at $Re_\tau = 4200$ with emphasis on the attached-eddy hypothesis, Phys. Rev. Fluids **2**, 014603 (2017).
[30] Y. Yamamoto and Y. Tsuji, Numerical evidence of logarithmic regions in channel flow at $Re_\tau = 8000$, Phys. Rev. Fluids **3**, 012602(R) (2018).
[31] C. Cheng, W. Li, A. Lozano-Durán, and H. Liu, Identity of attached eddies in turbulent channel flows with bidimensional empirical mode decomposition, J. Fluid Mech. **870**, 1037 (2019).
[32] M. K. Lee and R. D. Moser, Spectral analysis of the budget equation in turbulent channel flows at high Reynolds number, J. Fluid Mech. **860**, 886 (2019).

[33] A. Lozano-Durán and H. J. Bae, Characteristic scales of Townsend's wall-attached eddies, J. Fluid Mech. **868**, 698 (2019).
[34] A. Mehrez, J. Philip, Y. Yamamoto, and Y. Tsuji, Pressure and spanwise velocity fluctuations in turbulent channel flows: Logarithmic behavior of moments and coherent structures, Phys. Rev. Fluids **4**, 044601 (2019).
[35] S. Pirozzoli, J. Romero, M. Fatica, R. Verzicco, and P. Orlandi, One-point statistics for turbulent pipe flow up to $Re_\tau \approx 6000$, J. Fluid Mech. **926**, A28 (2021).
[36] C. Cheng and L. Fu, Consistency between the attached-eddy model and the inner-outer interaction model: A study of streamwise wall-shear stress fluctuations in a turbulent channel flow, J. Fluid Mech. **942**, R9 (2022).
[37] J. Yao, S. Rezaeiravesh, P. Schlatter, and F. Hussain, Direct numerical simulation of turbulent pipe flow up to $Re_\tau = 5200$, J. Fluid Mech. **956**, A18 (2023).
[38] Y. Hwang, Statistical structure of self-sustaining attached eddies in turbulent channel flow, J. Fluid Mech. **767**, 254 (2015).
[39] Y. Hwang and Y. Bengana, Self-sustaining process of minimal attached eddies in turbulent channel flow, J. Fluid Mech. **795**, 708 (2016).
[40] B. J. McKeon, Self-similar hierarchies and attached eddies, Phys. Rev. Fluids **4**, 082601(R) (2019).
[41] Q. Yang, A. P. Willis, and Y. Hwang, Exact coherent states of attached eddies in channel flow, J. Fluid Mech. **862**, 1029 (2019).
[42] Y. Hwang and B. Eckhardt, Attached eddy model revisited using a minimal quasi-linear approximation, J. Fluid Mech. **894**, A23 (2020).
[43] G. Wu, L. Fang, and J. Zhang, Numerical investigation and parametric analysis of an attached eddy model applied to inlet condition, Phys. Fluids **34**, 115143 (2022).
[44] G. Katul and B. Vidakovic, The partitioning of attached and detached eddy motion in the atmospheric surface layer using Lorentz wavelet filtering, Boundary-Layer Meteorol. **77**, 153 (1996).
[45] W. J. Baars and I. Marusic, Data-driven decomposition of the streamwise turbulence kinetic energy in boundary layers. Part 1. Energy spectra, J. Fluid Mech. **882**, A25 (2020).
[46] M. Yoon, J. Hwang, J. Yang, and H. J. Sung, Wall-attached structures of streamwise velocity fluctuations in an adverse-pressure-gradient turbulent boundary layer, J. Fluid Mech. **885**, A12 (2020).
[47] L.-W. Wang, C. Pan, J.-J. Wang, and Q. Gao, Statistical signatures of u component wall-attached eddies in proper orthogonal decomposition modes of a turbulent boundary layer, J. Fluid Mech. **944**, A26 (2022).
[48] M. Yu, C. X. Xu, J. Q. Chen, P. X. Liu, Y. L. Fu, and X. X. Yuan, Spectral decomposition of wall-attached/detached eddies in compressible and incompressible turbulent channel flows, Phys. Rev. Fluids **7**, 054607 (2022).
[49] C. M. de Silva, N. Hutchins, and I. Marusic, Uniform momentum zones in turbulent boundary layers, J. Fluid Mech. **786**, 309 (2016).
[50] R. J. Adrian, Hairpin vortex organization in wall turbulence, Phys. Fluids **19**, 041301 (2007).
[51] R. Baidya, J. Philip, N. Hutchins, J. P. Monty, and I. Marusic, Distance-from-the-wall scaling of turbulent motions in wall-bounded flows, Phys. Fluids **29**, 020712 (2017).
[52] C. M. de Silva, K. Kevin, R. Baidya, N. Hutchins, and I. Marusic, Large coherence of spanwise velocity in turbulent boundary layers, J. Fluid Mech. **847**, 161 (2018).
[53] C. M. de Silva, J. D. Woodcock, N. Hutchins, and I. Marusic, Influence of spatial exclusion on the statistical behavior of attached eddies, Phys. Rev. Fluids **1**, 022401(R) (2016).
[54] F. Eich, C. M. de Silva, I. Marusic, and C. J. Kähler, Towards an improved spatial representation of a boundary layer from the attached eddy model, Phys. Rev. Fluids **5**, 034601 (2020).
[55] D. Chandran, J. P. Monty, and I. Marusic, Spectral-scaling-based extension to the attached eddy model of wall turbulence, Phys. Rev. Fluids **5**, 104606 (2020).
[56] R. Deshpande, C. M. de Silva, M. Lee, J. P. Monty, and I. Marusic, Data-driven enhancement of coherent structure-based models for predicting instantaneous wall turbulence, Int. J. Heat Fluid Flow **92**, 108879 (2021).

[57] X. I. A. Yang, I. Marusic, and C. Meneveau, Moment generating functions and scaling laws in the inertial layer of turbulent wall-bounded flows, J. Fluid Mech. **791**, R2 (2016).
[58] X. I. A. Yang, I. Marusic, and C. Meneveau, Hierarchical random additive process and logarithmic scaling of generalized high order, two-point correlations in turbulent boundary layer flow, Phys. Rev. Fluids **1**, 024402 (2016).
[59] X. I. A. Yang and C. Meneveau, Hierarchical random additive model for wall-bounded flows at high Reynolds numbers, Fluid Dyn. Res. **51**, 011405 (2019).
[60] X. I. A. Yang, R. Baidya, P. Johnson, I. Marusic, and C. Meneveau, Structure function tensor scaling in the logarithmic region derived from the attached eddy model of wall-bounded turbulent flows, Phys. Rev. Fluids **2**, 064602 (2017).
[61] M. W. Ge, X. I. A. Yang, and I. Marusic, Velocity probability distribution scaling in wall-bounded flows at high Reynolds numbers, Phys. Rev. Fluids **4**, 034101 (2019).
[62] P. R. Spalart and J. H. Watmuff, Experimental and numerical study of a turbulent boundary layer with pressure gradients, J. Fluid Mech. **249**, 337 (1993).
[63] J.-H. Lee and H. J. Sung, Structures in turbulent boundary layers subjected to adverse pressure gradients, J. Fluid Mech. **639**, 101 (2009).
[64] Z. Harun, J. Monty, R. Mathis, and I. Marusic, Pressure gradient effects on the large-scale structure of turbulent boundary layers, J. Fluid Mech. **715**, 477 (2013).
[65] V. Kitsios, C. Atkinson, J. A. Sillero, G. Borrell, A. G. Gungor, J. Jiménez, and J. Soria, Direct numerical simulation of a self-similar adverse pressure gradient turbulent boundary layer, Int. J. Heat Fluid Flow **61**, 129 (2016).
[66] A. Bobke, R. Vinuesa, R. Örlü, and P. Schlatter, History effects and near equilibrium in adverse-pressure-gradient turbulent boundary layer, J. Fluid Mech. **820**, 667 (2017).
[67] R. Vinuesa, P. S. Negi, A. Atzori, A. Hanifi, D. S. Henningson, and P. Schlatter, Turbulent boundary layers around wing sections up to $Re_c = 1,000,000$, Int. J. Heat Fluid Flow **72**, 86 (2018).
[68] A. Tanarro, R. Vinuesa, and P. Schlatter, Effect of adverse pressure gradients on turbulent wing boundary layers, J. Fluid Mech. **883**, A8 (2020).
[69] R. Pozuelo, Q. Li, P. Schlatter, and R. Vinuesa, An adverse-pressure-gradient turbulent boundary layer with nearly constant $\beta \simeq 1.4$ up to $Re_\theta \simeq 8700$, J. Fluid Mech. **939**, A34 (2022).
[70] S. K. Robinson, Coherent motions in the turbulent boundary layer, Annu. Rev. Fluid Mech. **23**, 601 (1991).
[71] J. Jiménez, Coherent structures in wall-bounded turbulence, J. Fluid Mech. **842**, P1 (2018).
[72] L. Wang, R. Hu, and X. Zheng, A scaling improved inner-outer decomposition of near-wall turbulent motions, Phys. Fluids **33**, 045120 (2021).
[73] H. Mouri, Two-point correlation in wall turbulence according to the attached-eddy hypothesis, J. Fluid Mech. **821**, 343 (2017).
[74] X. I. A. Yang, R. Baidya, Y. Lv, and I. Marusic, Hierarchical random additive model for the spanwise and wall-normal velocities in wall-bounded flows at high Reynolds numbers, Phys. Rev. Fluids **3**, 124606 (2018).
[75] V. Kitsios, A. Sekimoto, C. Atkinson, J. A. Sillero, G. Borrell, A. G. Gungor, J. Jiménez, and J. Soria, Direct numerical simulation of a self-similar adverse pressure gradient turbulent boundary layer at the verge of separation, J. Fluid Mech. **829**, 392 (2017).
[76] A. Lozano-Durán, O. Flores, and J. Jiménez, The three-dimensional structure of momentum transfer in turbulent channels, J. Fluid Mech. **694**, 100 (2012).
[77] C. Cheng, W. Li, A. Lozano-Durán, and H. Liu, Uncovering Townsend's wall-attached eddies in low-Reynolds-number wall turbulence, J. Fluid Mech. **889**, A29 (2020).
[78] C. Cheng, W. Li, A. Lozano-Durán, and H. Liu, On the structure of streamwise wall-shear stress fluctuations in turbulent channel flows, J. Fluid Mech. **903**, A29 (2020).
[79] C. M. de Silva, D. Chandran, R. Baidya, N. Hutchins, and I. Marusic, Periodicity of large-scale coherence in turbulent boundary layers, Int. J. Heat Fluid Flow **83**, 108575 (2020).
[80] R. Hu, X. Zheng, and S. Dong, Extracting discrete hierarchies of Townsend's wall-attached eddies, Phys. Fluids **34**, 061701 (2022).

[81] W. J. Baars, N. Hutchins, and I. Marusic, Spectral stochastic estimation of high-Reynolds-number wall-bounded turbulence for a refined inner-outer interaction model, Phys. Rev. Fluids **1**, 054406 (2016).
[82] F. Moisy and J. Jiménez, Geometry and clustering of intense structures in isotropic turbulence, J. Fluid Mech. **513**, 111 (1999).
[83] J. C. del Álamo, J. Jiménez, P. Zandonade, and R. D. Moser, Self-similar vortex clusters in the turbulent logarithmic region, J. Fluid Mech. **561**, 329 (2006).
[84] S. Dong, A. Lozano-Durán, A. Sekimoto, and J. Jiménez, Coherent structures in statistically stationary homogeneous shear turbulence, J. Fluid Mech. **816**, 167 (2017).
[85] J. Hwang and H. J. Sung, Wall-attached structures of velocity fluctuations in a turbulent boundary layer, J. Fluid Mech. **856**, 958 (2018).
[86] L.-H. Wang, C.-X. Xu, H. J. Sung, and W.-X. Huang, Wall-attached structures over a traveling wavy boundary: Turbulent velocity fluctuations, Phys. Rev. Fluids **6**, 034611 (2021).
[87] J. Graham, K. Kanov, X. I. A. Yang, M. Lee, N. Malaya, C. C. Lalescu, R. Burns, G. Eyink, A. Szalay, R. D. Moser, and C. Meneveau, A web services accessible database of turbulent channel flow and its use for testing a new integral wall model for LES, J. Turbul. **17**, 181 (2016).
[88] L. Guastoni, A. Güemes, A. Ianiro, S. Discetti, P. Schlatter, H. Azizpour, and R. Vinuesa, Convolutional-network models to predict wall-bounded turbulence from wall quantities, J. Fluid Mech. **928**, A27 (2021).
[89] B. B. Mandelbrot, *The Fractal Geometry of Nature* (Freeman, New York, 1982).
[90] K. R. Sreenivasan, Fractals and multifractals in fluid turbulence, Annu. Rev. Fluid Mech. **23**, 539 (1991).
[91] H. H. A. Xu and X. I. A. Yang, Fractality and the law of the wall, Phys. Rev. E **97**, 053110 (2018).
[92] I. Marusic, W. J. Baars, and N. Hutchins, Scaling of the streamwise turbulence intensity in the context of inner-outer interactions in wall turbulence, Phys. Rev. Fluids **2**, 100502 (2017).
[93] X. Chen and K. Sreenivasan, Reynolds number scaling of the peak turbulence intensity in wall flows, J. Fluid Mech. **908**, R3 (2021).
[94] X. Chen and K. Sreenivasan, Law of bounded dissipation and its consequences in turbulent wall flows, J. Fluid Mech. **933**, A20 (2022).
[95] N. Skouloudis and Y. Hwang, Scaling of turbulence intensities up to $Re_\tau = 10^6$ with a resolvent-based quasilinear approximation, Phys. Rev. Fluids **6**, 034602 (2021).
[96] A. J. Smits, M. Hultmark, M. Lee, S. Pirozzoli, and X. Wu, Reynolds stress scaling in the near-wall region of wall-bounded flows, J. Fluid Mech. **926**, A31 (2021).
[97] A. J. Smits, B. J. McKeon, and I. Marusic, High-Reynolds number wall turbulence, Annu. Rev. Fluid Mech. **43**, 353 (2011).
[98] C. Meneveau and I. Marusic, Generalized logarithmic law for high-order moments in turbulent boundary layers, J. Fluid Mech. **719**, R1 (2013).
[99] I. Marusic, R. Mathis, and N. Hutchins, Predictive model for wall-bounded turbulent flow, Science **329**, 193 (2010).
[100] R. Mathis, N. Hutchins, and I. Marusic, A predictive inner-outer model for streamwise turbulence statistics in wall-bounded flows, J. Fluid Mech. **681**, 537 (2011).
[101] J. M. Hamilton, J. Kim, and F. Waleffe, Regeneration mechanisms of near-wall turbulence structures, J. Fluid Mech. **287**, 317 (1995).
[102] J. Jiménez and A. Pinelli, The autonomous cycle of near-wall turbulence, J. Fluid Mech. **389**, 335 (1999).
[103] W. Schoppa and F. Hussain, Coherent structure generation in near-wall turbulence, J. Fluid Mech. **453**, 57 (2002).
[104] S. Hoyas and J. Jiménez, Scaling of the velocity fluctuations in turbulent channels up to $Re_\tau = 2003$, Phys. Fluids **18**, 011702 (2006).
[105] R. Hu and X. Zheng, Energy contributions by inner and outer motions in turbulent channel flows, Phys. Rev. Fluids **3**, 084607 (2018).
[106] L. Wang and R. Hu, Inner-outer decomposition of wall shear stress fluctuations in turbulent channels, Theor. Appl. Mech. Lett. **12**, 100337 (2022).
[107] Z. Xia, G. Brethouwer, and S. Chen, High-order moments of streamwise fluctuations in a turbulent channel flow with spanwise rotation, Phys. Rev. Fluids **3**, 022601(R) (2018).

[108] P. A. Davidson, T. B. Nickels, and P.-Å. Krogstad, The logarithmic structure function law in wall-layer turbulence, J. Fluid Mech. **550**, 51 (2006).

[109] C. M. de Silva, I. Marusic, J. D. Woodcock, and C. Meneveau, Scaling of second-and higher-order structure functions in turbulent boundary layers, J. Fluid Mech. **769**, 654 (2015).

[110] J.-H. Xie, C. de Silva, R. Baidya, X. I. A. Yang, and R. Hu, Third-order structure function in the logarithmic layer of boundary-layer turbulence, Phys. Rev. Fluids **6**, 074602 (2021).